Available online at www.sciencedirect.com

SciVerse ScienceDirect

journal homepage: www.elsevier.com/locate/he

The effect of the blockage ratio on the blow-off limit of a hydrogen/air flame in a planar micro-combustor with a bluff body

Aiwu Fan [a,*], Jianlong Wan [a], Yi Liu [a], Boming Pi [a], Hong Yao [a], Kaoru Maruta [b], Wei Liu [a]

[a] State Key Laboratory of Coal Combustion, Huazhong University of Science and Technology, 1037 Luoyu Road, Wuhan 430074, China

[b] Institute of Fluid Science, Tohoku University, Sendai 980-8577, Japan

ARTICLE INFO

Article history:
Received 8 May 2013
Received in revised form
21 June 2013
Accepted 22 June 2013
Available online 23 July 2013

Keywords:
Micro-combustor
Blow-off limit
Blockage ratio
Recirculation zone
Stretching effect
Heat loss

ABSTRACT

We recently developed a micro-combustor with a bluff body, which has a demonstrated 3- to 5-time extension in the blow-off limit. In the present work, the dimension effect of the bluff body on the blow-off limit (indicated by the blockage ratio, ζ) was investigated with a detailed H_2/O_2 reaction mechanism. The results indicate that the blow-off limits for $\zeta = 0.3$, 0.4 and 0.5 are 20, 31 and 36 m/s, respectively. Analyses reveal that for $\zeta = 0.3$, flame blowout occurs due to insufficient recirculation zone size. However, flame blowout occurs due to the stretching effect in the shear layers when $\zeta = 0.4$ and 0.5. Calculations indicate that the three cases have negligible differences in heat loss because the high temperature zones are located in the combustor centers; therefore, their effects on the combustor walls are mitigated.

1. Introduction

With the fast development of micro-electro-mechanic system (MEMS) technology, various micro- and meso-scale devices and systems, such as micro gas turbines, propulsion systems, robots and portable electric devices, are continuously emerging. Conventional batteries have several disadvantages, such as short life spans, long recharging periods and low energy densities. Combustion-based micro-power sources are considered a competitive alternative to batteries, particularly due to their use of hydrocarbon fuels, which results in significantly higher energy densities [1,2]. The micro-combustor is a key component of micro-power generation systems. This component converts the chemical energy of fuels into thermal energy through combustion. Thus, the development of micro-combustors with a wide and stable operational range has attracted increasing attention over the last decade.

However, maintaining stable combustion in a micro-combustor is challenging. The increased heat loss and wall radical capture due to the large surface area-to-volume ratio make it difficult to sustain a stable flame at small scales [1–3].

* *Corresponding author*. Tel.: +86 27 87542618; fax: +86 27 87540724.
E-mail addresses: faw@hust.edu.cn, faw_73@163.com (A. Fan).

0360-3199/$ – see front matter
http://dx.doi.org/10.1016/j.ijhydene.2013.06.100

Another critical problem is the shortened residence time of the gaseous mixture in the combustor. Many unstable flames have been reported to date [4–11]. For instance, flames with repetitive extinction and ignition (FREI) of a premixed methane/air mixture were observed in both straight channels and curved ducts [4,5]. This combustion mode was later numerically reproduced by other researchers [6,7]. In addition, Kumar et al. [8,9] and Fan et al. [10–15] observed some special flame patterns, such as a rotating spiral-like flame, in a heated radial micro-channel.

Considerable efforts have been made to improve the flame stability in micro- and meso-scale combustors. Thermal management methods, such as heat recirculation and heat loss control, are good ways to overcome the negative effect of heat loss and thus sustain a stable flame in small devices [16–21]. The "Swill-roll" structure is a good example of heat recirculation that has been implemented to stabilize flames in micro- and meso-scale combustors [16–19]. The combustion characteristics of premixed H_2/air in a planar micro-combustor with a stainless steel mesh were experimentally studied by Li et al. [20]. These researchers' work indicated that flames can be effectively anchored by the inserted porous media. Jiang et al. [21] developed a miniature cylindrical combustor with a porous wall that could effectively stabilize the flame in the combustor chamber by reducing the heat loss and preheating the cold feed mixture.

In addition, catalytic combustion is an excellent way to stabilize flames at small scales because the catalyst can accelerate the reaction and suppress radical depletion at the wall [22,23]. Boyarko et al. [24] investigated the catalytic combustion of a hydrogen/oxygen mixture in platinum tubes with internal diameters of 0.4 mm and 0.8 mm for micro-propulsion applications. Zhou et al. [25] studied catalytic micro-combustors made of quartz, alumina ceramic and copper through experimental observations and CFD simulations. Their results showed that these three combustors perform differently. Choi et al. [26] investigated the combustion characteristics of a sub-millimeter catalytic combustor with a platinum catalyst on a porous ceramic support. The results of this study showed that catalytic combustion is applicable to sub-millimeter scale combustors. Di Benedetto et al. [27,28] studied a micro-combustor which was divided into two parts: a first catalytic part and a second non-catalytic part. The results show that this scheme allows operating at high inlet velocity and maintaining high combustion efficiency. In addition, they investigated the effect of cross-sectional geometry on the thermal behavior of catalytic micro-combustors. It demonstrates that the square cross-section micro-rector is more resistant to extinction than the cylindrical channel. Kaisare et al. [29] analyzed the stability and performance of platinum-catalyzed micro-reactors for lean propane-air combustion. It is found that the transverse heat and mass transport strongly depend on the inlet flow rate and the thermal conductivity of the solid material. Karagiannidis et al. [30] investigated the hetero-/homogeneous steady combustion and the stability limits in methane-fueled catalytic micro-reactor. The results showed that the stability limits of catalytic micro-reactors were wider than those reported for non-catalytic systems.

Utilizing the recirculation zone of the flow field is another effective way to stabilize flames in micro-combustors. Yang et al. [31] and Pan et al. [32] developed micro-combustors with a backward-facing step. Their experimental results showed that this step is useful to control the flame position and widen several operational ranges, namely the inlet velocity and the H_2/air ratio. Khandelwal et al. [33] investigated the flame stability of premixed methane/air in micro-combustors with two backward steps. Their results showed that flames can be stable for wide ranges of the inlet velocity and equivalence ratio. Wan et al. [34] developed a micro-combustor with a bluff body that can extend the blow-off limit by 5-fold over the straight-channel combustor. The recirculation zone and shear layers are widely known to affect the flame stability in the bluff body combustor. The bluff body dimension (indicated by the blockage ratio, ζ) significantly influences the characteristics of the flow field and thus the flame stabilization in the micro-combustor. For the present work, we numerically investigated the dimension effect of the bluff body on the blow-off limit of premixed H_2/air flames. The underlying mechanisms are discussed with respect to the flow field near the bluff body and the heat loss from the outer walls.

2. Numerical methods

2.1. Geometrical model

Fig. 1 schematically shows the longitudinal cross-section of the bluff body micro-combustor. The total length of the combustor (L_0) is 16.0 mm. The width (W_0) and height (W_1) of the combustor chamber are 10 mm and 1 mm, respectively. The thickness of combustor wall (W_3) is 1 mm. The cross-sectional area of the bluff body is an equilateral triangle, which is symmetrical with respect to the upper and lower walls. The distance from the vertical surface of the bluff body

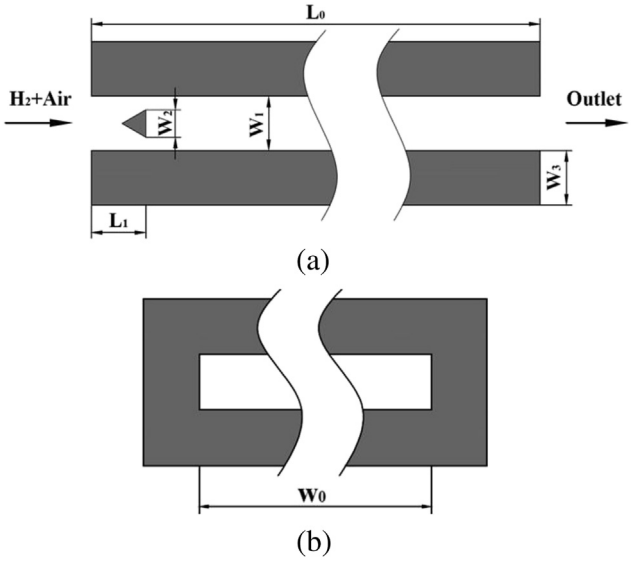

Fig. 1 – Schematic diagram of the micro-combustor with a bluff body: (a) longitudinal cross-section of the combustor, (b) combustor exit.

to the combustor inlet (L_1) is 1 mm. The dimension of the bluff body is indicated by the blockage ratio, a dimensionless parameter defined as $\zeta = W_2/W_1$, in which W_2 is the side length of the bluff body.

2.2. Mathematical model

Because the characteristic length of the combustor chamber is still notably larger than the molecular mean-free path of the gases that flow through the micro-combustor, fluids can be reasonably treated as continuums. Therefore, the Navier–-Stokes equations are still applicable to the present study [35]. However, the mixing of various species in the micro-combustor is enhanced by the small space and large concentration gradients. Therefore, turbulence models are expected to better reflect the strengthened mixing and its effect on combustion characteristics than the laminar model. This expectation has been confirmed by several researchers [17,34,36]. For example, Zhang et al. [36] reported that the turbulence model predicts the experimental data better than the laminar model. Kuo and Ronney [17] also suggest that turbulence models more appropriately estimate the combustion characteristics in micro-combustors when the Reynolds number is above approximately 500. For our combustor, the inlet velocity that corresponds to $Re = 500$ is approximately 8.0 m/s. The bluff body micro-combustor's primary purpose is to extend the blow-off limit, which is much larger than 8.0 m/s (refer to subsection 3.2). Furthermore, we have compared several turbulence models and found that the realizable k-epsilon model is the best, i.e., the numerically predicted blow-off limit based on the realizable k-epsilon model agreed reasonably well with our experimental data [34]. Therefore, we apply the same model in the present study. In addition, according to Ref. [37], the standard wall function is still applicable when the Reynolds number is larger than 150. For our cases, the Reynolds numbers are respectively 382, 510 and 636 for the blockage ratios of 0.3, 0.4 and 0.5 at an inlet velocity of 10 m/s. Therefore, the standard wall function is suitable for the present work and was adopted to solve the near-wall zone. Because the heat conduction in the solid wall may significantly affect combustion [17], the computations presented in this study address the heat transfer in both of the combustor walls and the bluff body.

2.3. Computation scheme

Hydrogen and air were selected as the fuel and oxidant, respectively. The density of the gas mixture was calculated using the ideal gas assumption, while the specific heat, viscosity and thermal conductivity were calculated from a mass fraction weighted average of the species' properties. Quartz was used as the solid material. The temperature dependences of the thermal conductivity (λ) and the specific heat capacity (c_p) of the solid material were incorporated using polynomial functions based on handbook values [38], as shown in Eqs. (1) and (2).

$$\lambda = 4.7\times10^{-12}T^4 - 1.2\times10^{-8}T^3 + 1.2\times10^{-5}T^2 - 4.4\times10^{-3}T + 1.7 \quad (1)$$

$$c_p = -2.7\times10^{-7}T^3 + 3.6\times10^{-4}T^2 + 0.45T + 5.9\times10^{2} \quad (2)$$

where the T is the temperature of the solid material.

The reaction mechanism reported by Li et al. [39] was applied to model the combustion of H_2/air mixtures. It consists of 13 species and 19 reversible elementary reactions. The thermodynamic and transport properties of the gaseous species could be found in the CHEMKIN databases [40,41]. Because the micro-combustor had been specially processed to ensure the inertness of all interior surfaces, the surface reaction effect was not considered in the CFD simulation.

The uniform concentration and velocity distributions of the premixed H_2/air mixture were specified at the inlet of the micro-combustor. The equivalence ratio of the mixture was fixed at 0.5. The inlet temperature of mixture was set to 300 K. An outflow boundary condition was specified at the exit. The effects of surface to surface radiation between the inner surfaces of the combustor were considered using the discrete ordinates (DO) model [17]. A non-slip and a zero species flux normal to the wall surfaces boundary condition were applied at the inner walls. At the outer surfaces of the solid walls, the total heat loss via both natural convection and thermal radiation to the surroundings was calculated using Eq. (3):

$$Q' = hA(T_{W,O} - T_\infty) + \varepsilon\sigma A\left(T_{W,O}^4 - T_\infty^4\right) \quad (3)$$

where h is the natural convection heat transfer coefficient (20 W/(m^2 K)) [42], $T_{w,o}$ is the outer wall temperature, T_∞ is the ambient temperature (300 K), A is the exterior surface area of the combustor, ε is the emissivity of the solid surface with a value of 0.92, and σ is the Stephan–Boltzmann constant, 5.67×10^{-8} W/(m^2 K^4).

The computational fluid dynamics (CFD) software package FLUENT 6.3 [43] was applied to solve the mass, momentum, energy and species conservation equations as well as the conjugated heat conduction in solid materials. The second-order upwind scheme was used to discretize the model, and the "SIMPLE" algorithm was employed to couple the pressure and the velocity. Because the aspect ratio (W_0/W_1) of the combustor chamber is very large (10:1), we adopted a two-dimensional model for our numerical simulations to reduce the computation load. The results were verified to be grid-independent, and a non-uniform square grid system was employed in the computation. The convergence of the CFD simulation was judged based on the residuals of all governing equations. The results obtained in this study were achieved with residuals smaller than 1.0×10^{-6}.

3. Results and discussion

3.1. Model validation

The numerical model presented in this study was validated in a previous study by experimental data [34] (Fig. 2). Fig. 2 shows that the predicted blow-off limits agree reasonably well with their experimental counterparts. The relative errors between the numerical and experimental results are 5.3%, 12.2% and 5.8% for equivalence ratios of 0.4, 0.5 and 0.6, respectively. This finding confirms that the numerical model adopted in the present study is reasonably accurate.

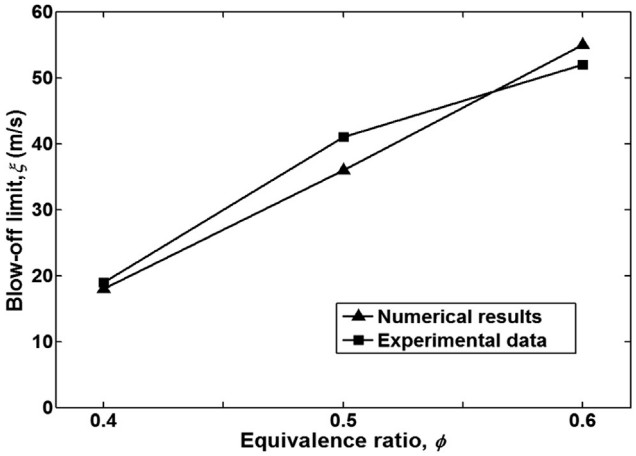

Fig. 2 – Experimental and numerical results for blow-off limits in the bluff body micro-combustor with a blockage ratio of 0.5 [34].

3.2. *Effect of the blockage ratio on the blow-off limit*

Blow-off limit values (ξ) for various blockage ratios (ζ) of the bluff body combustors are shown in Fig. 3. This figure indicates that the blow-off limits for $\zeta = 0.3$, 0.4 and 0.5 are 20 m/s, 31 m/s and 36 m/s, respectively. In other words, the blow-off limit correlates positively with the blockage ratio.

The flame stability in the bluff body micro-combustor was expected to be affected by both the flow field and heat loss. For the convenience of discussion, we define the area where the longitudinal velocity component $V_x \leq 0$ as the recirculation zone. The length of this recirculation zone is defined as the longest distance from the contour of $V_x = 0$ to the right wall of bluff body. Similarly, the heat-loss ratio, Φ, is defined in Eq. (4) to indicate the ratio of heat loss from the outer walls, Q', to the input enthalpy involved in the fuel, Q.

$$\Phi = Q'/Q \tag{4}$$

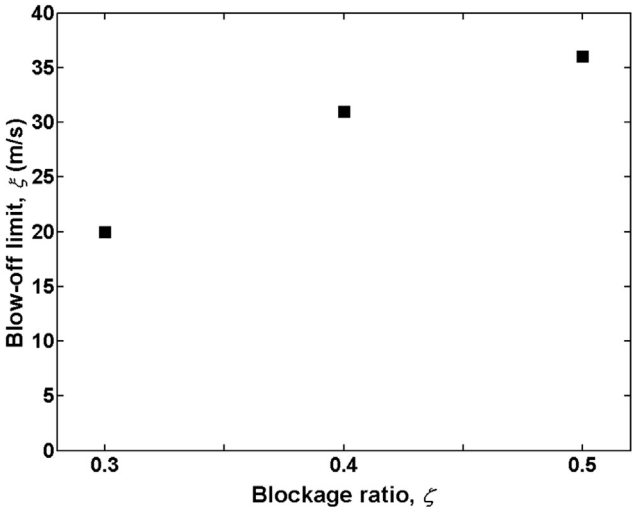

Fig. 3 – Blow-off limits for micro-combustors with a bluff body at different blockage ratios and an equivalence ratio of 0.5.

In addition, as pointed out by Schmitt [44], although the Boussinesq's turbulent viscosity hypothesis are widely used for many applications, it is always invalid for complex flows, high mixing rates, recirculation regions and so on. This has been verified by both numerical and experimental data [44]. Therefore, the turbulent viscosity extracted from the Fluent results are inappropriate to compute the shear stress and thus we use the horizontal and vertical velocity components to qualitatively analyze the stretch effect based on the velocity gradients, $\partial v/\partial x$ and $\partial u/\partial y$, in the shear layers. A detailed discussion of these parameters will follow.

3.3. *Discussion*

3.3.1. *Effect of the flow field*

Fig. 4 shows the contours of the longitudinal velocity component in the bluff body combustors for different blockage ratios. An increase in the recirculation zone area and length is to be expected with an increase in bluff body dimension. This increase can clearly be seen in Fig. 4.

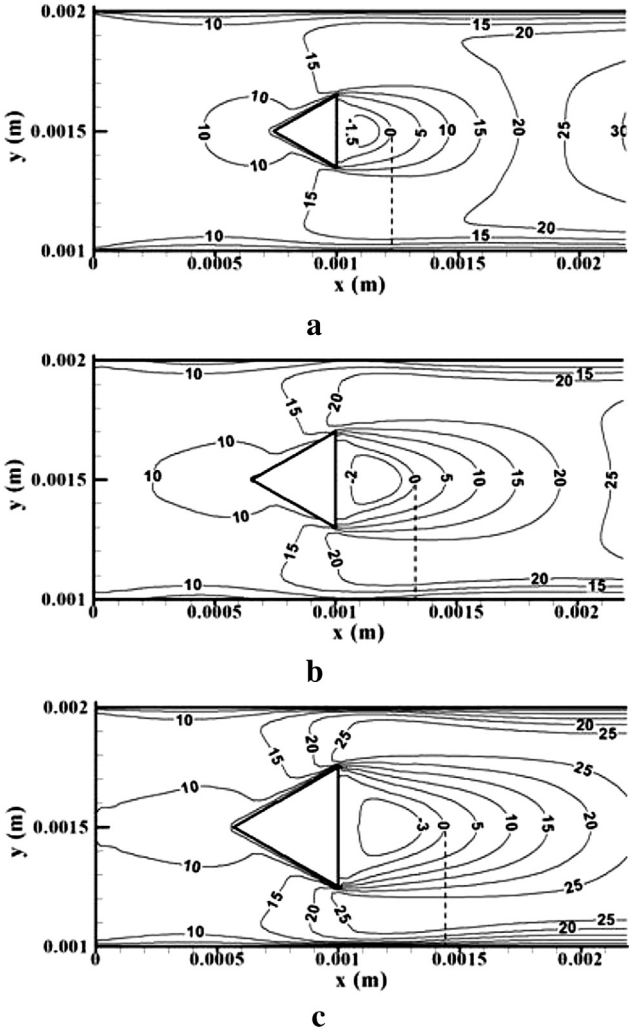

Fig. 4 – Contours of the longitudinal velocity component near the bluff body ($0 < x < 0.0022$ m) at an inlet velocity of 10 m/s: (a) $\zeta = 0.3$, (b) $\zeta = 0.4$, (c) $\zeta = 0.5$.

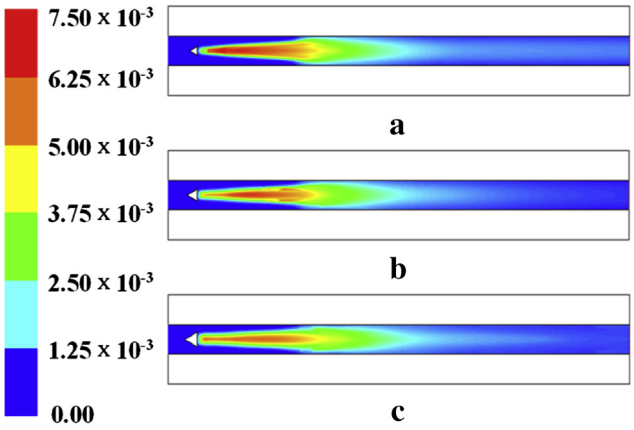

Fig. 5 – Mass fraction contours for the –OH radicals in the bluff body combustors at an inlet velocity of 10 m/s: (a) $\zeta = 0.3$, (b) $\zeta = 0.4$, (c) $\zeta = 0.5$.

The recirculation zone is crucial to stabilize the flame in the bluff body combustor because it not only provides a low-velocity region to anchor the flame root, but it also generates a pool of certain key radicals, such as H and OH. Fig. 5 presents the complete high temperature zones (indicated by the mass fraction contours of radical OH) of the three cases. The inlet velocities are the same for each case (10 m/s). For the convenience of comparison, local distributions of radical OH ($0 < x < 0.0022$ m) are also shown in Fig. 6, where the right boundary of the recirculation zone is indicated by a dashed white line. Fig. 5 indicates that the peak value of the OH mass fraction is maximized at a blockage ratio of 0.3. However, Fig. 6 clearly shows that the peak OH concentration and the radical OH region in the recirculation zone are both minimized at this blocking ratio. Conversely, the area of high OH concentration in the recirculation zone is maximized when the blockage ratio is 0.5. Therefore, a blockage ratio of 0.5 provides the stablest flame and thus the largest blow-off limit among the three cases.

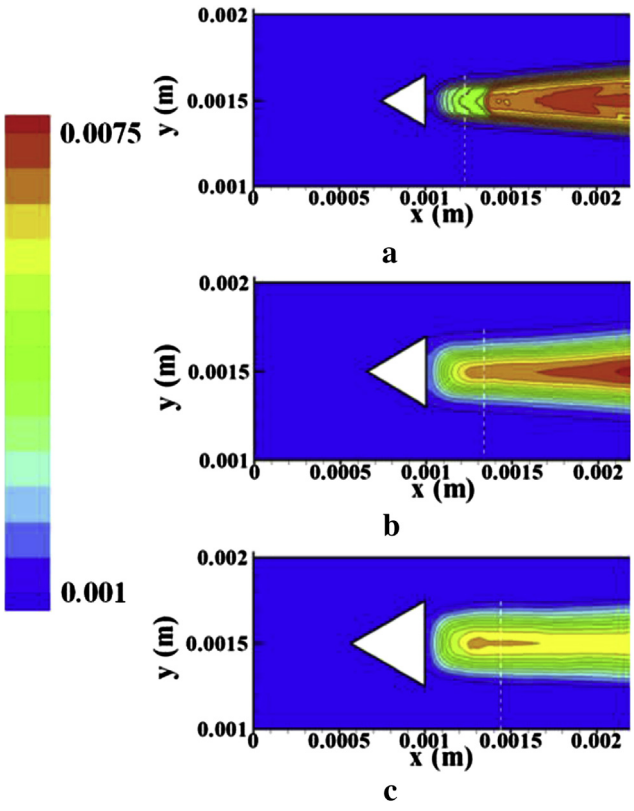

Fig. 6 – Mass fraction contours for the –OH radicals near the bluff body ($0 < x < 0.0022$ m) at an inlet velocity of 10 m/s: (a) $\zeta = 0.3$, (b) $\zeta = 0.4$, (c) $\zeta = 0.5$.

To reveal the mechanisms that underlie flame blowout in the three cases, the high temperature zones (indicated by the mass fraction contours of radical OH) near the blow-off limits are shown in Fig. 7. This figure shows that the high temperature zones are prolonged under near-limit conditions for all three cases. However, the shape of high temperature zone differs from the other two cases when the blockage ratio is 0.3. Specifically, the high temperature zone remains intact at high inlet velocities for this blockage ratio, but the concentration of radical OH is very low in the recirculation zone. This low concentration in the recirculation zone approximates the situation provided by low inlet velocities, such as that shown in Fig. 5a. In contrast, the high temperature zone is almost split in two near the blow-off limit at blockage ratios of 0.4 and 0.5. The OH concentration in the recirculation zone is comparatively lower, and the corresponding area is much narrower than that of its high temperature zone counterpart. When the inlet velocity is slightly increased beyond this scenario, the two high temperature zones will be totally separated, and the smaller one that is located in the recirculation zone cannot solely sustain the flame. Consequently, the flame is blown out. This phenomenon was also observed in our previous experimental investigation, as shown for the first time in Fig. 8. This photograph was taken directly with a digital camera at the blow-off limit condition for a micro-combustor with a blockage ratio of 0.5. This picture shows

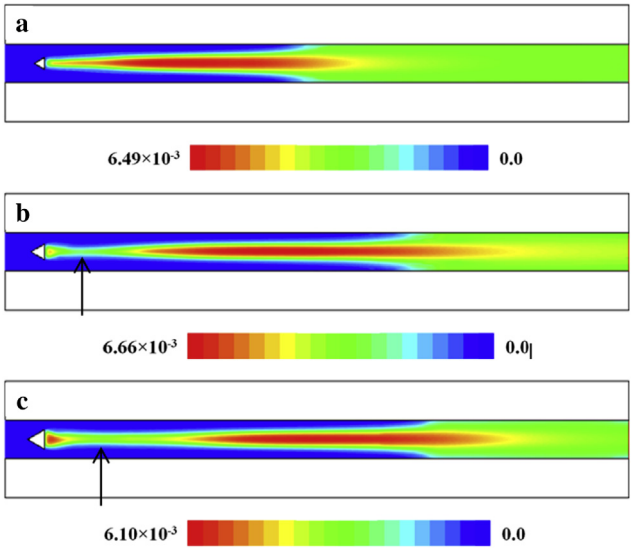

Fig. 7 – Mass fraction contours for the –OH radicals at blow-off limit conditions: (a) $\zeta = 0.3$ and inlet velocity = 20 m/s; (b) $\zeta = 0.4$ and inlet velocity = 31 m/s; (c) $\zeta = 0.5$ and inlet velocity = 36 m/s.

Fig. 8 – Flame photograph directly taken with a digital camera in our experiment at the blow-off limit.

that the flame is split in two prior to blowout, which likely results from a stretching effect caused by the shear layers. To elucidate this hypothesis, we present the contours of the vertical velocity component near the bluff body ($0 < x < 0.0022$ mm) in Fig. 9. In each case, the locations of the shear layers are indicated by two arrows. It is evident from Figs. 4 and 9 that the shear stress strengthens when the blockage ratio is increased from 0.3 to 0.5 because the velocity gradients, $\partial u/\partial y$ and $\partial v/\partial x$, in the shear layers grow increasingly larger.

The above discussion indicates that at a blockage ratio of 0.3, the flame is blown out at a comparatively lower limit because the recirculation zone is too small. Conversely, the flame roots can be anchored at relatively higher inlet velocities for blockage ratios of 0.4 and 0.5 due to sufficiently large recirculation zones. In these cases, blowout eventually occurs due to flame stretching, which arises from the large shear stress that results from very high inlet velocities.

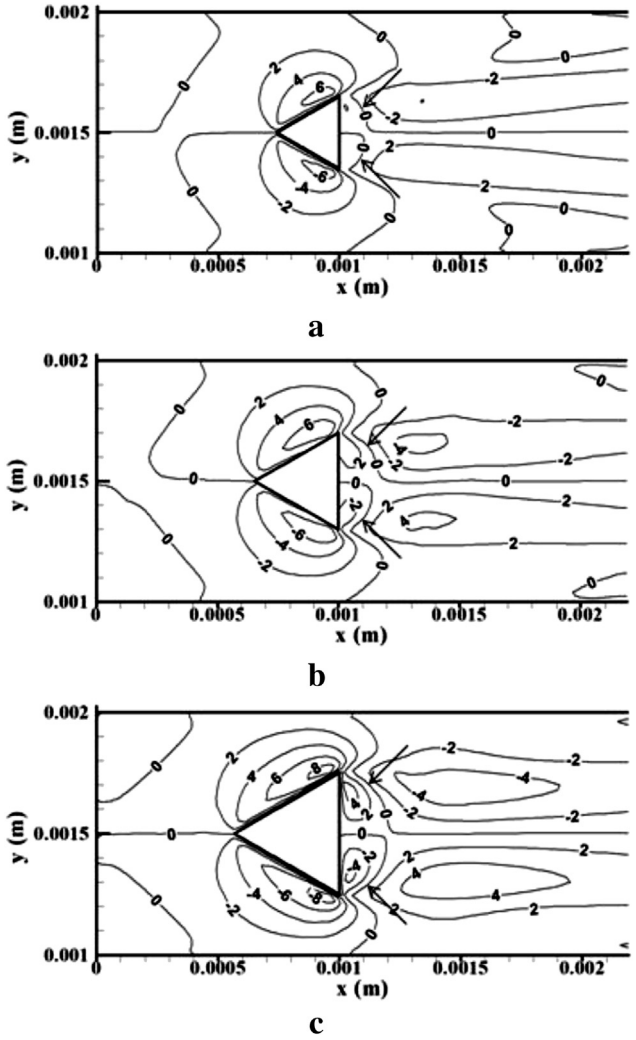

Fig. 9 – Contours of the vertical velocity component near the bluff body ($0 < x < 0.0022$ m) at an inlet velocity of 10 m/s: (a) $\zeta = 0.3$, (b) $\zeta = 0.4$, (c) $\zeta = 0.5$.

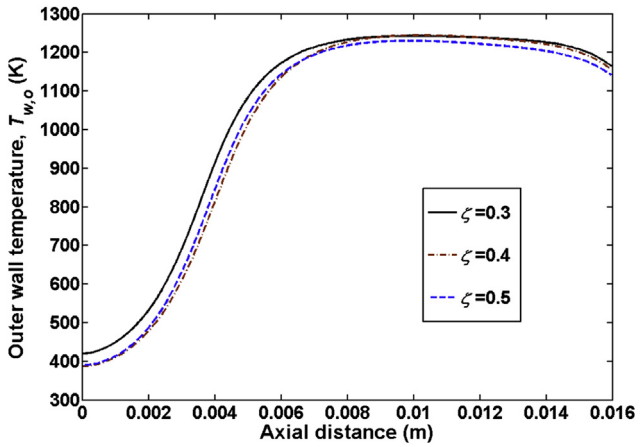

Fig. 10 – Outer wall temperature profiles for the bluff body combustors at different blockage ratios and an inlet velocity of 10 m/s.

3.3.2. *Effect of heat loss*

Fig. 10 illustrates the outer wall temperature profiles of the combustors for different blockage ratios at an inlet velocity of 10 m/s. As evident from the figure, the differences between the three cases are limited. This lack of difference can primarily be attributed to the high temperature zone that lies symmetrically to the upper and lower walls in the center of the bluff body combustor chamber (Fig. 5). The shapes of the high temperature zones have a direct effect on the temperature fields of the three cases, as shown in Fig. 11. This figure indicates that the three temperature fields are similar and only the parts in the recirculation zones differ slightly.

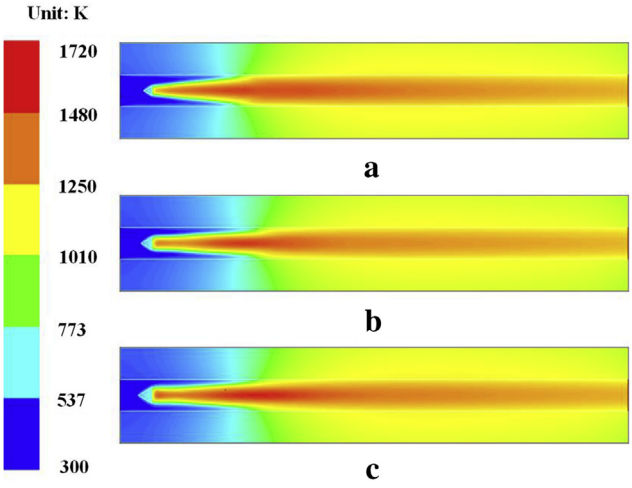

Fig. 11 – Temperature fields of the three combustors at an inlet velocity of 10 m/s: (a) $\zeta = 0.3$, (b) $\zeta = 0.4$, (c) $\zeta = 0.5$.

The heat-loss ratios (including the convective heat-loss ratio Φ_{con}, the radiation heat-loss ratio Φ_{rad} and the total heat-loss ratio Φ_{tot}) of the three combustors were obtained based on the computation results. The results show that the convective heat-loss ratios for the blockage ratios of 0.3, 0.4 and 0.5 are 3.77%, 3.63% and 3.61%, respectively, while the corresponding radiation heat-loss ratios are 21.39%, 20.46% and 19.59%, respectively. The total heat-loss ratios for the blockage ratios of 0.3, 0.4 and 0.5 are 25.16%, 24.09% and 23.2%, respectively. These data reveal that the total heat-loss ratio is slightly reduced when the blockage ratio is increased. Specifically, the maximum difference in the total heat-loss ratio among the three cases is only 1.96%. This indicates that the differences in the heat loss have a negligible effect on the differences among the blow-off limits of the three combustors. Furthermore, the results demonstrate that the heat-loss ratio attributed to radiation is much larger than that attributed to convection. This radiation dominance results from relatively high outer wall temperatures because radiation strongly depends on the wall temperature ($\propto (T_{w,o}^4 - T_\infty^4)$).

4. Conclusions

The effect of the bluff body dimension on the blow-off limit of a planar micro-combustor was investigated by numerical simulations. The results show that the blow-off limits for combustors with blockage ratios of 0.3, 0.4 and 0.5 are 20 m/s, 31 m/s and 36 m/s, respectively. These values were obtained for an equivalence ratio of 0.5 in all cases. The analyses were conducted with respect to the flow field near the bluff body and the heat loss from the outer walls. They revealed that the recirculation zone generates a pool of key radicals with low-velocity and thus dominates flame stabilization for combustors with a bluff body. However, blow-out was facilitated by different mechanisms for the three cases. When the blockage was 0.3, the flame was blown out at a comparatively lower limit because the recirculation zone was too small. Because the recirculation zones are wider for micro-combustors with blockage ratios of 0.4 and 0.5, they can sustain a flame at comparatively higher inlet velocities. However, the stretching effect in the shear layers is enhanced when the flow areas are reduced on both sides of the bluff body. Thus, the flame is blown out if the inlet velocity is increased further. The heat-loss analysis shows that the differences in heat-loss ratios among the three cases are negligible. This is because the high temperature zones are located at the centers of the combustor chambers, which mitigates their effects on the combustor walls.

Acknowledgments

This work was supported by the Natural Science Foundation of China (Grant Nos. 51076054 and 51276073), and the Foundation of Key Laboratory of Low-grade Energy Utilization Technologies and Systems, Chongqing University, China.

REFERENCES

[1] Fernandez-Pello AC. Micro-power generation using combustion: issues and approaches. Proc Combust Inst 2002;29:883–99.
[2] Maruta K. Micro and mesoscale combustion. Proc Combust Inst 2011;33:125–50.
[3] Li JW, Zhong BJ. Experimental investigation on heat loss and combustion in methane/oxygen micro-tube combustor. Appl Therm Eng 2008;28:707–16.
[4] Maruta K, Kataoka T, Kim NI, Minaev S, Fursenko R. Characteristics of combustion in a narrow channel with a temperature gradient. Proc Combust Inst 2005;30:2429–36.
[5] Richecoeur F, Kyritsis DC. Experimental study of flame stabilization in low Reynolds and Dean number flows in curved mesoscale ducts. Proc Combust Inst 2005;30:2419–27.
[6] Jackson TL, Buckmaster J, Lu Z, Kyritsis DC, Massa L. Flames in narrow circular tubes. Proc Combust Inst 2007;31:955–62.
[7] Minaev S, Maruta K, Fursenko R. Nonlinear dynamics of flame in a narrow channel with a temperature gradient. Combust Theory Model 2007;11:187–203.
[8] Kumar S, Maruta K, Minaev S. Pattern formation of flames in radial microchannels with lean methane-air mixtures. Phys Rev E 2007;75:016208.
[9] Kumar S, Maruta K, Minaev S. On the formation of multiple rotating pelton-like flame structures in radial microchannels with lean methane-air mixtures. Proc Combust Inst 2007;31:3261–8.
[10] Fan AW, Minaev S, Kumar S, Liu W, Maruta K. Regime diagrams and characteristics of flame patterns in radial microchannels. Combust Flame 2008;153:479–89.
[11] Fan AW, Minaev S, Sereshchenko E, Fursenko R, Kumar S, Liu W, et al. Experimental and numerical investigations of flame pattern formations in a radial microchannel. Proc Combust Inst 2009;32:3059–66.
[12] Fan AW, Minaev S, Kumar S, Liu W, Maruta K. Experimental study on flame pattern formation and combustion completeness in a radial microchannel. J Micromech Microengin 2007;17:2398–406.
[13] Fan AW, Maruta K, Nakamura H, Kumar S, Liu W. Experimental investigation on flame pattern formations of DME–air mixtures in a radial microchannel. Combust Flame 2010;157:1637–42.
[14] Fan AW, Wan JL, Maruta K, Nakamura H, Yao H, Liu W. Flame dynamics in a heated meso-scale radial channel. Proc Combust Inst 2013;34:3351–9.
[15] Fan AW, Maruta K, Nakamura H, Liu W. Experimental investigation of flame pattern transitions in a heated radial micro-channel. Appl Therm Eng 2012;47:111–8.
[16] Sitzki L, Borer K, Wussow S, Schuster E, Maruta K, Ronney PD, et al. Combustion in microscale heat-recirculating burners. In: AIAA-2001-1078, 39th AIAA space sciences & exhibit, Reno, NV; 2001.
[17] Kuo CH, Ronney PD. Numerical modeling of non-adiabatic heat-recirculating combustors. Proc Combust Inst 2007;31:3277–84.
[18] Kim NI, Kato S, Kataoka T, Yokomori T, Maruyama S, Fujimori T, et al. Flame stabilization and emission of small Swiss-roll combustors as heaters. Combust Flame 2005;141:229–40.
[19] Zhong BJ, Wang JH. Experimental study on premixed CH_4/air mixture combustion in micro Swiss-roll combustors. Combust Flame 2010;157:2222–9.
[20] Li J, Chou SK, Li ZW, Yang WM. Experimental investigation of porous media combustion in a planar micro-combustor. Fuel 2010;89:708–15.

[21] Jiang LQ, Zhao DQ, Wang XH, Yang WB. Development of a self-thermal insulation miniature combustor. Energ Convers Manage 2009;50:1308–13.
[22] Chen GB, Chen CP, Wu CY, Chao YC. Effects of catalytic walls on hydrogen/air combustion inside a micro-tube. Appl Catal A Gen 2007;332:89–97.
[23] Chao YC, Chen GB, Hsu CJ, Leu TS, Wu CY, Cheng TS. Operational characteristics of catalytic combustion in a platinum micro tube. Combust Sci Tech 2004;176:1755–77.
[24] Boyarko GA, Sung CJ, Schneider SJ. Catalyzed combustion of hydrogen-oxygen in platinum tubes for micro-propulsion applications. Proc Combust Inst 2005;30:2481–8.
[25] Zhou JH, Wang Y, Yang WJ, Liu JZ, Wang ZH, Cen KF. Combustion of hydrogen–air in catalytic micro-combustors made of different material. Int J Hydrogen Energy 2009;34:3535–45.
[26] Choi WY, Kwon SJ, Shin H. Combustion characteristics of hydrogen-air premixed gas in a sub-millimeter scale catalytic combustor. Int J Hydrogen Energy 2008;33:2400–8.
[27] Di Benedetto A, Di Sarli V, Russo G. A novel catalytic-homogenous micro-combustor. Catal Today 2009;147S:156–61.
[28] Di Benedetto A, Di Sarli V, Russo G. Effect of geometry on the thermal behavior of catalytic micro-combustors. Catal Today 2010;155:116–22.
[29] Kaisare NS, Deshmukh SR, Vlachos DG. Stability and performance of catalytic microreactors: simulations of propane catalytic combustion on Pt. Chem Eng Sci 2008;63:1098–116.
[30] Karagiannidis S, Mantzaras J, Jackson G, Boulouchos K. Hetero-/homogeneous combustion and stability maps in methane-fueled catalytic microreactors. Proc Combust Inst 2007;31:3309–17.
[31] Yang WM, Chou SK, Shu C, Li ZW, Xue H. Combustion in micro-cylindrical combustors with and without a backward facing step. Appl Therm Eng 2002;22:1777–87.
[32] Pan JF, Huang J, Li DT, Yang WM, Tang WX, Xue H. Effects of major parameters on micro-combustion for thermophotovoltaic energy conversion. Appl Therm Eng 2007;27:1089–95.
[33] Khandelwal B, Sahota GPS, Kumar S. Investigations into the flame stability limits in a backward step micro scale combustor with premixed methane-air mixtures. J Micromech Microeng 2010;20:095030.
[34] Wan JL, Fan AW, Maruta K, Yao H, Liu W. Experimental and numerical investigation on combustion characteristics of premixed hydrogen/air flame in a micro-combustor with a bluff body. Int J Hydrogen Energy 2012;37:19190–7.
[35] Beskok A, Karniadakis GE. A model for flows in channels, pipes, and ducts at micro and nano scales. Microscale Therm Eng 1999;3:43–77.
[36] Zhang YS, Zhou JH, Yang WJ, Liu MS, Cen KF. Study on the model selection for micro-combustion simulation. Proc Chin Soc Elect Eng 2006;26:81–7 [in Chinese].
[37] Daly BJ, Harlow FH. Transport equations in turbulence. Phys Fluids 1970;13:2634–49.
[38] Ma QF, Fang RS, Xiang LC. Handbook of thermo-physical properties. Bejing: China Agricultural Machinery Press; 1986 [in Chinese].
[39] Li J, Zhao ZW, Kazakov A, Dryer FL. An updated comprehensive kinetic model of hydrogen combustion. Int J Chem Kinet 2004;36:1–10.
[40] Kee RJ, Rupley FM, Miller JA. The CHEMKIN thermodynamic database. Sandia National Laboratories Report SAND87–8215B 1990.
[41] Kee RJ, Grear JF, Smooke MD, Miller JA. A Fortran program for modeling steady laminar one-dimensional premixed flames. Sandia National Laboratories Report SAND85–8240 1985.
[42] Holman JP. Heat transfer. 9th ed. New York: McGraw-Hill; 2002.
[43] Fluent 6.3 user's guide. Lebanon, New Hampshire: Fluent Inc.; 2006.
[44] Schmitt FG. About Boussinesq's turbulence viscosity hypothesis: historical remarks and a direct evaluation of its validity. C R Mecanique 2007;335:617–27.